E1-2003-163

D. V. Bandurin[1], N. B. Skachkov[2]

SETTING THE ABSOLUTE SCALE OF JET ENERGY WITH «Z^0 + jet» EVENTS AT LHC

[1]E-mail: dvm@cv.jinr.ru
[2]E-mail: skachkov@cv.jinr.ru

1. Introduction

A precise reconstruction of the jet energy is an extremely important task in many experiments of high energy physics. The previous studies of possibilities to apply for this aim different physical processes (like "$Z^0/\gamma + jet$" and others), done in D0, CDF, CMS and ATLAS collaborations may be found in [1]–[16].

"$Z^0 + jet$" events with one high-P_t jet can provide an useful sample to perform *in situ* determination of a jet transverse momentum via the transverse momentum of Z^0 boson reconstructed from the precisely measured leptonic Z^0 decay ($Z^0 \to \mu^+\mu^-, e^+e^-$).

In this paper we limit our consideration to $Z^0 \to \mu^+\mu^-$ decay only. The amount of material in front and inside the muon detector system guarantees absorbing most hadronic background. Besides, by using the track segments matching between the muon system and the tracker one can reach a high enough reconstruction efficiency of a muon track with a good momentum resolution (of order of $0.5 - 1\%$) [17].

"$Z^0 + jet$" events is an useful tool to cross-check a setting an absolute jet energy scale with help of other processes like "$\gamma + jet$" [12]–[16] and "$W \to 2\ jets$" events [8], for example.

Here we present results of the analysis of "$Z^0 + jet$" events generated by using PYTHIA 5.7 Monte-Carlo event simulation package [18].

2. Generalities of the "$Z^0 + jet$" process

2.1 Leading order picture and sources of P_t^Z and P_t^{jet} imbalance

In this section we observe briefly the main effects that lead to the imbalance between P_t^Z and P_t^{jet}.

The process of $Z^0 + jet$ production

$$pp \to Z^0 + 1\,jet + X \qquad (1)$$

is caused at the parton level by two subprocesses: Compton-like scattering

$$qg \to q + Z^0 \qquad (2a)$$

and the annihilation process

$$q\bar{q} \to g + Z^0. \qquad (2b)$$

If the initial state radiation (ISR) is absent, the total transverse momentum of the final state in the subprocesses (2a) or (2b) is equal to zero, i.e. the P_t balance equation for Z^0 and final parton would look as

$$\vec{P_t}^{Z+part} = \vec{P_t}^{Z} + \vec{P_t}^{part} = 0. \qquad (3)$$

Thus, having neglected hadronization effect we could expect that a jet transverse momentum P_t^{jet} is close enough to Z^0 boson transverse momentum, i.e. $\vec{P_t}^{jet} \approx -\vec{P_t}^{Z}$.

A radiation of a gluon in the initial state with a non-zero transverse momentum $P_t^{gluon} \equiv P_t^{ISR} \neq 0$ can produce a imbalance between P_t^Z and P_t^{part} and, thus, between transverse momenta of Z^0 boson and the jet originated from this proton. The corresponding next-to-leading order diagrams are shown in Fig. 2. Some leading order Feynman diagrams of these processes are shown in Fig. 1.

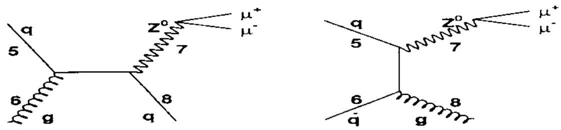

Fig. 1: Some leading order Feynman diagrams for Z^0 production.

Following [12], we choose the sum of the modulus of the transverse momentum vectors $\vec{P_t}^5$ and $\vec{P_t}^6$ of the incoming (into $2 \to 2$ fundamental QCD subprocesses $5 + 6 \to 7 + 8$) partons (lines 5 and 6 in Fig. 2):

$$P_t56 = |P_t^5| + |P_t^6| \tag{4}$$

as a quantitative measure to estimate the P_t imbalance caused by ISR.

The numerical notations in the Feynman diagrams shown in Figs. 1 and 2 and in formula (4) are chosen to be in correspondence with those used in the PYTHIA event listing for description of the parton–parton subprocess.

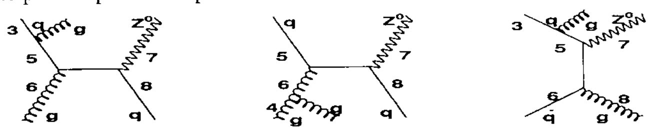

Fig. 2: Some Feynman diagrams of Z^0 production including gluon radiation in the initial state.

Let us consider fundamental subprocesses in which there is no initial state radiation but instead final state radiation (FSR) takes place. Some Feynman diagrams of the signal subprocesses with the FSR are shown in Fig. 3. An appearance of a gluon in the final state may also cause a imbalance between transverse momenta of Z^0 and jet. But because it manifests itself as some extra jets or clusters, like in the case of ISR, the same selection criteria (see below) as for suppression of ISR can be used.

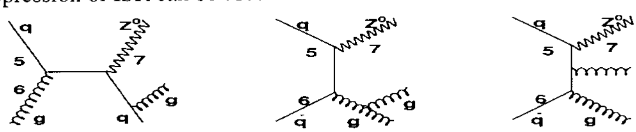

Fig. 3: Some of Feynman diagrams of Z^0 production including gluon radiation in the final state.

A possible non-zero value of the intrinsic transverse momentum of a parton inside a colliding proton (k_T) may be another source of the $P_t{}^Z$ and $P_t{}^{part}$ imbalance in the final state. Its reasonable value is supposed to lead to the value of $k_T \leq 1.0\, GeV/c$. Below we shall keep the value of k_T to be fixed by the PYTHIA default value $\langle k_T \rangle = 0.44\, GeV/c$. The dependence of the imbalance between $P_t{}^Z$ and $P_t{}^{Jet}$ on a possible variation of k_T is discussed in detail in [16, 21]. The general conclusion is that the variation of k_T within reasonable boundaries does not produce a large effect when the initial state radiation is taken into account. The latter makes a dominant contribution.

Another non-perturbative effect that results in the $P_t{}^Z$ and $P_t{}^{jet}$ imbalance is an hadronization of the parton, produced in the fundamental $2 \to 2$ subprocess, into a jet. The contribution of the hadronization to this imbalance is calculated within the Lund string fragmentation scheme used by default in PYTHIA. The mean values of the relative $P_t{}^{Jet} - P_t{}^{part}$ imbalance are presented in Appendix to [22] for three different jetfinders, UA1, UA2 and LUCELL, as a function of the variable which limit a cluster activity beyond the "$Z^0 + jet$" system (see Section 2.2 and [14]).

contribution of the hadronization to this imbalance is calculated within the Lund string fragmentation scheme used by default in PYTHIA. The mean values of the relative ${P_t}^{Jet} - {P_t}^{part}$ imbalance are presented in Appendix to [22] for three different jetfinders, UA1, UA2 and LUCELL, as a function of the variable which limit a cluster activity beyond the "$Z^0 + jet$" system (see Section 2.2 and [14]).

2.2 Definition of selection cuts

1. We shall select the events with Z^0 boson [1] and one jet with

$$ {P_t}^Z \geq 40\, GeV/c \quad \text{and} \quad {P_t}^{jet} \geq 30\, GeV/c. \tag{5}$$

For most of our applications the jet is defined according to the PYTHIA jetfinding algorithm LUCELL. The jet cone radius R in the $\eta - \phi$ space counted from the jet initiator cell (ic) is taken to be $R_{ic} = ((\Delta\eta)^2 + (\Delta\phi)^2)^{1/2} = 0.7$.

2. To guarantee a clear identification of a muon track from Z^0 decay in the muon and tracker systems and determination of its parameters we put the following restrictions on muons [2]:

(a) on the P_t value of any considered muon:

$$ {P_t}^\mu \geq 10\, GeV/c; \tag{6}$$

(b) on the P_t value of the most energetic muon in a pair:

$$ P^\mu_{t\,max} \geq P^\mu_{t\,CUT} \tag{7}$$

($P^\mu_{t\,CUT} \geq 20\, GeV/c$ and depends on the energy scale; see Fig. 6 of Section 3.2);

(c) on the value of the ratio of ${P_t}^{isol}$, i.e. the scalar sum of P_t of all particles surrounding a muon, to ${P_t}^\mu$ (${P_t}^{isol}/{P_t}^\mu$) in the cone of radius $R = 0.3$ and on the value of maximal P_t of a charged particle surrounding a muon in this cone:

$$ {P_t}^{isol}/{P_t}^\mu \leq 0.10, \quad {P_t}^{ch} \leq 2\, GeV/c. \tag{8}$$

The isolated high-P_t tracks can be reconstructed with a good efficiency (at least 98% over all pseudorapidity region $|\eta| < 2.4$; see [17]) and with generation of a low number of fake and ghost tracks.

3. A muon is selected in the acceptance region of the muon system:

$$ |\eta^\mu| < 2.4. \tag{9}$$

4. To select muon pairs only from the Z^0 decay we limit the value of invariant mass of a muon pair M^{ll}_{inv} by:

$$ |M^Z - M^{ll}_{inv}| \leq 5\, GeV/c^2. \tag{10}$$

5. We select the events with the vector $\vec{P_t}^{jet}$ being "back-to-back" to the vector $\vec{P_t}^{Z}$ (in the plane transverse to the beam line) within $\Delta\phi$ defined by the equation:

$$ \phi_{(Z,jet)} = 180^\circ \pm \Delta\phi \tag{11}$$

---

[1] Here and below in the paper speaking about Z^0 boson we imply a signal reconstructed from the muon pair with muons selected by the criteria $2 - 4$ of this section.

[2] Most of the muon selection cuts are taken from [17, 19].

where $\phi_{(Z,jet)}$ is the angle between vectors $\vec{P_t}^Z$ and $\vec{P_t}^{jet}$: $\vec{P_t}^Z \vec{P_t}^{jet} = P_t^Z P_t^{jet} cos(\phi_{(Z,jet)})$, with $P_t^Z = |\vec{P_t}^Z|$, $P_t^{jet} = |\vec{P_t}^{jet}|$. The angle $\Delta\phi$ defined in the interval $5 \div 15^\circ$ is the most effective choice.

6. The initial and final state radiations (ISR and FSR) manifest themselves most clearly as some final state mini-jets or clusters activity (see the previous section and [12]–[16]). To suppress it, we impose a new cut condition that was not formulated in an evident form in previous experiments: we choose the "$Z^0 + jet$" events that do not have any other jet-like or cluster high P_t activity by taking values of P_t^{clust} (with the cluster cone of $R_{clust}(\eta, \phi) = 0.7$), being smaller than some threshold P_{tCUT}^{clust} value, i.e. we select the events with

$$P_t^{clust} \leq P_{tCUT}^{clust}. \tag{12}$$

7. We limit the value of the modulus of the vector sum of $\vec{P_t}$ of all particles that do not belong to the "$Z^0 + jet$" system but fit into the region $|\eta| < 5$ covered by the calorimeter system, i.e., we limit the signal in the cells "beyond the jet and Z^0" regions by the following cut:

$$\left| \sum_{i \notin jet, Z^0} \vec{P_t}^i \right| \equiv P_t^{out} \leq P_{tCUT}^{out}, \quad |\eta| < 5. \tag{13}$$

The importance of P_{tCUT}^{out} and P_{tCUT}^{clust} for selection of events with a good balance of P_t^Z and P_t^{jet} was already shown in [12] – [16] and in [21].

The set of selection cuts 1 – 7 we call below as "Selection 1".

8. By analogy with [12] – [16] and [21] we use a "jet isolation" requirement (introduced for the first time in [12]), i.e. the presence of a "clean enough" (in the sense of limited P_t activity) region inside the ring of $\Delta R = 0.3$ around the jet. Following this picture, we restrict the ratio of the scalar sum of transverse momenta of particles belonging to this ring, i.e.

$$P_t^{ring}/P_t^{jet} \equiv \epsilon^{jet}, \quad \text{where} \quad P_t^{ring} = \sum_{i \in 0.7 < R < 1} |\vec{P_t}^i| \tag{14}$$

with $\epsilon^{jet} \leq 3 - 8\%$ (see Sections 6 and 7).

The set of cuts that 1 – 8 will be called "Selection 2".

9. As we have shown in [12, 21] one can expect reasonable results of modeling the jet energy calibration procedure and subsequent practical realization only if one uses a set of selected events with small missing transverse momentum P_t^{miss}. We define it here as a P_t vector sum of all the particles flying mostly in the direction of the non-instrumented region $|\eta| > 5.0$ and neutrinos with $|\eta| < 5.0$:

$$\vec{P_t}^{miss} = \vec{P_t}^{|\eta|>5.0} + \sum_{i \in |\eta| < 5.0} \vec{P}^i_{t(\nu)}. \tag{15}$$

Here $\vec{P_t}^{|\eta|>5}$ is the total transverse momentum of non-observable particles i flying in the direction of the non-instrumented forward part of the CMS detector ($|\eta| > 5$):

$$\sum_{i \in |\eta| > 5} \vec{P_t}^i \equiv \vec{P_t}^{|\eta|>5}. \tag{16}$$

So, we shall use the following cut on P_t^{miss}:

$$P_t^{miss} \leq P_{tCUT}^{miss}. \tag{17}$$

The exact values of the cut parameters P_{tCUT}^{μ}, ϵ^{jet}, P_{tCUT}^{clust}, P_{tCUT}^{out} will be specified below, since they may be different, for instance, for various ${P_t}^Z$ intervals.

2.3 The P_t-balance equation of "$Z^0 + jet$" event.

The conservation law for "$Z^0 + jet$" events as a whole can be written in the following vector form [12, 21]:

$$\vec{P_t}^{Z} + \vec{P_t}^{jet} + \vec{P_t}^{O} + \vec{P_t}^{|\eta|>5} = 0. \tag{18}$$

$\vec{P_t}^{|\eta|>5}$ is defined in (16) and $\vec{P_t}^{O}$ is a total transverse momentum of all other (O) particles besides "jet particles and muons from Z^0 decay" ("$Z^0 + jet$" system) in the $|\eta| < 5$ region and defined as:

$$\vec{P_t}^{O} = \vec{P_t}^{out} + \vec{P}^{O}_{t(\nu)} + \vec{P}^{O}_{t(\mu,|\eta^\mu|>2.4)}. \tag{19}$$

In its turn, $\vec{P_t}^{out}$ is a sum of clusters P_t (with ${P_t}^{clust}$ smaller than ${P_t}^{jet}$) and P_t of single hadrons (h), photons (γ) and electrons (e) with $|\eta| < 5$ and muons (μ) with $|\eta^\mu| < 2.4$ that are out of the "$Z^0 + jet$" system:

$$\vec{P_t}^{out} = \vec{P_t}^{clust} + \vec{P}^{sing}_{t(h)} + \vec{P}^{nondir}_{t(\gamma)} + \vec{P}_{t(e)} + \vec{P}^{O}_{t(\mu,|\eta^\mu|<2.4)}, \quad |\eta| < 5. \tag{20}$$

The last two terms in equation (19) are the transverse momentum carried out by the neutrinos that do not belong to the jet but that are contained in the $|\eta| < 5$ region ($\vec{P}^{O}_{t(\nu)}$) and non-detectable muons flying with $|\eta^\mu| > 2.4$ ($\vec{P}^{O}_{t(\mu,|\eta^\mu|>2.4)}$).

To conclude this section, let us rewrite the basic vector P_t-balance equation in the following scalar form, more suitable to present the final results:

$$\frac{{P_t}^Z - {P_t}^{jet}}{{P_t}^Z} = (1 - cos\Delta\phi) + P_t(O{+}\eta > 5)/{P_t}^Z, \tag{21}$$

where $P_t(O{+}\eta > 5) \equiv (\vec{P_t}^{O} + \vec{P_t}^{|\eta|>5}) \cdot \vec{n}^{jet}$ with $\vec{n}^{jet} = \vec{P_t}^{jet}/{P_t}^{jet}$ and $\Delta\phi$ is the angle that enters equation (11).

As will be shown in Section 4, the first term on the right-hand side of equation (21) is negligibly small and tends to decrease fast with growing ${P_t}^{jet}$. So, the main contribution to the P_t imbalance in the "$Z^0 + jet$" system is caused by the term $P_t(O{+}\eta > 5)/{P_t}^Z$ [12]–[16], [21].

3. Event rates for different ${P_t}^Z$ and η^Z intervals.

3.1 Dependence of the distribution of the number of events on the "back-to-back" angle $\phi_{(Z,jet)}$ and on ${P_t}^{ISR}$.

Here we study the spectrum of the variable P_t56 for the sample of signal events [3]. For this aim four samples of "$Z^0 + jet$" events (each by $5 \cdot 10^6$) were generated by using PYTHIA with subprocesses (2a) and (2b) and with minimal P_t of hard scattering [4] $2 \to 2$ $\hat{p}_{\perp}^{\,min} = 20, 35, 50, 75\ GeV/c$ to cover four ${P_t}^Z$ intervals: 40–50, 70–85, 100–120, 150–200 GeV/c, respectively. The obtained cross sections for these subprocesses are given in Table 1.

[3] P_t56 is approximately proportional to ${P_t}^{ISR}$ up to the value of intrinsic parton transverse momentum k_T inside a proton ($\langle k_T\rangle$ was taken to be fixed at the PYTHIA default value, i.e. $\langle k_T\rangle = 0.44\ GeV/c$).

[4] CKIN(3) parameter in PYTHIA [?]

Table 1: The cross sections (in $microbarns$) of the $qg \to q + Z^0$ and $q\bar{q} \to g + Z^0$ subprocesses for four $\hat{p}_{\perp}^{\,min}$ values.

Subprocess type	$\hat{p}_{\perp}^{\,min}$ values (GeV/c)			
	20	35	50	75
$qg \to q + Z^0$	$3.83 \cdot 10^{-4}$	$1.71 \cdot 10^{-4}$	$9.14 \cdot 10^{-5}$	$3.80 \cdot 10^{-5}$
$q\bar{q} \to g + Z^0$	$1.20 \cdot 10^{-4}$	$0.42 \cdot 10^{-4}$	$1.93 \cdot 10^{-5}$	$0.69 \cdot 10^{-5}$
Total	$5.03 \cdot 10^{-4}$	$2.13 \cdot 10^{-4}$	$1.11 \cdot 10^{-4}$	$4.59 \cdot 10^{-5}$

For our analysis we used cuts (5) – (13) and the following cut parameters:

$$P_{t\,max}^{\mu} > 20\ GeV/c, \quad \Delta\phi < 15^\circ, \quad P_{tCUT}^{clust} = 30\ GeV/c. \tag{22}$$

In Tables 2, 3 and 5, 6 we study (as in [12]) P_t56 spectra for two most illustrative cases of ${P_t}^Z$ intervals $40 < {P_t}^Z < 50\ GeV/c$ (Tables 2 and 5) and $100 < {P_t}^Z < 120\ GeV/c$ (Tables 3 and 6). The distributions of the number of events for the integrated luminosity $L_{int} = 10\,fb^{-1}$ in different P_t56 intervals and for different "back-to-back" angle intervals $\phi_{(Z,jet)} = 180^\circ \pm \Delta\phi$ (with $\Delta\phi = 15^\circ$, 10° and 5° as well as without any restriction on $\Delta\phi$, i.e. for the whole ϕ interval $\Delta\phi = 180^\circ$) are given there. The LUCELL jetfinder was used to find jets and clusters. Tables 2 and 3 correspond to the events selected with cuts ${P_t}^{clust} < 30\,GeV/c$ and without any limit on ${P_t}^{out}$ value, while Tables 5 and 6 correspond to more restrictive selection cuts ${P_t}^{clust} < 10\,GeV/c$ and ${P_t}^{out} < 10\,GeV/c$.

Firstly, from the last summary lines of Tables 2, 3 and 5, 6 we can make a general conclusion about the $\Delta\phi$ dependence of the event spectrum. In the case when no restriction is used we can see that for the $40 \le {P_t}^Z \le 50\ GeV/c$ (Table 2) interval about 65% of events are concentrated in the $\Delta\phi < 15^\circ$ range, while 30% of events are in the $\Delta\phi < 5^\circ$ range. At the same time the analogous summary line of Table 3 shows us that for $100 \le {P_t}^Z \le 120\,GeV/c$ the event spectrum moves noticeably to the small $\Delta\phi$ region: more than 94% of events have $\Delta\phi < 15^\circ$ and 56% of them have $\Delta\phi < 5^\circ$.

We observe a tendency of the distributions of the number of signal "$Z^0 + jet$" events to be concentrated in a rather narrow back-to-back angle interval $\Delta\phi < 15^\circ$ with ${P_t}^Z$ growing. It becomes more distinct with a more restrictive cuts $P_{tCUT}^{out} = 10\,GeV/c$ and $P_{tCUT}^{out} = 10\,GeV/c$ (Tables 5 and 6). From the last summary line of Table 5 we see for these cuts that in the case of $40 \le {P_t}^Z \le 50\,GeV/c$ more than 96% of the events have $\Delta\phi < 15^\circ$, while 60% of them are in the $\Delta\phi < 5^\circ$ range. For $100 \le {P_t}^Z \le 120\,GeV/c$ (see Table 6) more than 92% of the events, subject to these cuts, have $\Delta\phi < 5^\circ$. It means that while suppressing P_t activity beyond the "$Z^0 + jet$" system by imposing $P_{tCUT}^{clust} = 10\ GeV/c$ and $P_{tCUT}^{out} = 10\,GeV/c$ we can select the sample of events with a clean back-to-back ($\Delta\phi < 15^\circ$) topology of $\vec{P_t}^Z$ and $\vec{P_t}^{jet}$ orientation [5].

The other lines of Tables 2, 3 and 5, 6 contain the information about the P_t56 spectrum (or, up to k_T effect, ${P_t}^{ISR}$ spectrum).

From the comparison of Table 2 with Table 5 (as well as from Tables 3 and 6) one can conclude that *the width of the most populated part of the P_t56 (or ${P_t}^{ISR}$) spectrum is noticeably reduced with restricting P_{tCUT}^{clust} and P_{tCUT}^{out}.*

[5] An increase in ${P_t}^Z$ produces the same effect, as is seen from Tables 3 and 5, and is demonstrated in more detail in Section 4 and [22].

Table 2: Number of events dependence on P_t56 and $\Delta\phi$ for $40 \leq P_t{}^Z \leq 50\,GeV/c$ and $P_t{}^{clust}_{CUT} = 30\,GeV/c$ for L_{int}=10 fb^{-1}.

P_t56 (GeV/c)	$\Delta\phi_{max}$			
	180°	15°	10°	5°
0 – 5	18525	16965	15880	12708
5 – 10	29094	26671	23419	13579
10 – 15	24192	19935	14042	7033
15 – 20	18168	10910	7088	3481
20 – 25	13424	5833	3924	1968
25 – 30	10169	3604	2380	1172
30 – 40	14070	4114	2677	1311
40 – 50	7544	1833	1184	618
50 – 100	5904	1727	1097	550
100 – 300	8	3	2	0
300 – 500	0	0	0	0
30 – 500	141095	91594	71694	42423

Table 3: Number of events dependence on P_t56 and $\Delta\phi$ for $100 \leq P_t{}^Z \leq 120\,GeV/c$ and $P_t{}^{clust}_{CUT} = 30\,GeV/c$ for L_{int}=10 fb^{-1}.

P_t56 (GeV/c)	$\Delta\phi_{max}$			
	180°	15°	10°	5°
0 – 5	1849	1837	1790	1616
5 – 10	3798	3770	3667	3247
10 – 15	3635	3600	3477	2542
15 – 20	3065	3025	2847	1592
20 – 25	2491	2424	1976	986
25 – 30	2115	2000	1418	709
30 – 40	2507	2039	1398	721
40 – 50	1061	744	527	289
50 – 100	1105	768	582	325
100 – 300	194	147	107	63
300 – 500	2	2	1	0
0 – 500	21826	20356	17797	12094

Table 4: Number of events dependence on $\Delta\phi$ and on $P_t{}^Z$ for $L_{int} = 10\,fb^{-1}$. $P_t{}^{clust}_{CUT} = 30\,GeV/c$ (summary).

$P_t{}^Z$ (GeV/c)	$\Delta\phi_{max}$			
	180°	15°	10°	5°
40 – 50	141095	91591	71694	42423
70 – 80	40032	32551	26710	16794
100 – 120	2182	20356	17797	12094
150 – 200	8649	8558	8134	6182

Table 5: Number of events dependence on P_t56 and $\Delta\phi$ for $40 \le P_t{}^Z \le 50\, GeV/c$ and $Pt^{clust}_{CUT} = 10\ GeV/c$ and $Pt^{out}_{CUT} = 10\ GeV/c$ for L_{int}=10 fb^{-1}.

P_t56 (GeV/c)	$\Delta\phi_{max}$			
	180°	15°	10°	5°
0 – 5	11619	11603	11409	9603
5 – 10	15329	15258	14288	8767
10 – 15	6787	6479	5156	2768
15 – 20	1810	1533	1204	645
20 – 25	677	527	432	253
25 – 30	305	238	195	119
30 – 40	277	222	193	111
40 – 50	127	111	91	44
50 – 100	36	32	24	12
100 – 300	0	0	0	0
300 – 500	0	0	0	0
0 – 500	36967	35996	32987	22315

Table 6: Number of events dependence on P_t56 and $\Delta\phi$ for $100 \le P_t{}^Z \le 120\, GeV/c$ and $Pt^{clust}_{CUT} = 10\ GeV/c$ and $Pt^{out}_{CUT} = 10\ GeV/c$ for L_{int}=10 fb^{-1}.

P_t56 (GeV/c)	$\Delta\phi_{max}$			
	180°	15°	10°	5°
0 – 5	1133	1133	1133	1121
5 – 10	1932	1932	1932	1877
10 – 15	1002	1002	1002	867
15 – 20	309	309	309	234
20 – 25	95	95	91	63
25 – 30	49	49	45	33
30 – 40	48	44	40	32
40 – 50	27	25	25	25
50 – 100	44	44	44	40
100 – 300	5	5	5	5
300 – 500	0	0	0	0
0 – 500	4641	4637	4621	4293

Table 7: Number of events dependence on $\Delta\phi$ and on P_t^Z for $L_{int} = 10\ fb^{-1}$. $Pt^{clust}_{CUT} = 10\ GeV/c$ and $Pt^{out}_{CUT} = 10\ GeV/c$ (summary).

$P_t{}^Z$ (GeV/c)	$\Delta\phi_{max}$			
	180°	15°	10°	5°
40 – 50	36967	35996	32987	22315
70 – 80	8688	8657	8542	7033
100 – 120	4641	4637	4621	4293
150 – 200	1746	1746	1742	1719

$P_t{}^Z$ intervals and contain analogous numbers of events that can be collected in different $\Delta\phi$ intervals for P_{tCUT}^{clust}, P_{tCUT}^{out} and other cuts, defined by (22), at $L_{int} = 10\, fb^{-1}$.

We can conclude from Tables 2–7 that restriction on the P_{tCUT}^{clust} and P_{tCUT}^{out} variables are good tools to reduce ISR while by limiting $\Delta\phi$ angle the ISR remains, in fact, without a change. Meanwhile, in spite of about twofold spectra reduction of the ISR (or P_t56), see Tables 4 and 7, it continues to be noticeable at the LHC energies [6].

3.2 $P_t{}^Z$, η^Z and $P_t{}^\mu$ dependence of rates

In Table 8 we present the number of events calculated after passing selection cuts (5)–(13) for different $P_t{}^Z$ and η^Z intervals (lines and columns of the table, respectively). The last column of this table contains the total number of events (at $L_{int} = 10\, fb^{-1}$) at $|\eta^Z| < 5.0$ for a given $P_t{}^Z$ interval. We see that the number of events decreases fast with growing $P_t{}^Z$ (but it decreases much slower as compared with decrease in $P_t{}^\gamma$ spectrum in the case of "$\gamma + jet$" events, see [12]). It also drops with growing $|\eta^Z|$ starting from $|\eta^Z| \approx 2.0$ and has weak dependence on η^Z in the interval $|\eta^Z| < 2.0$. The analogous information is illustrated by Fig. 5 for three $P_t{}^Z$ intervals [7].

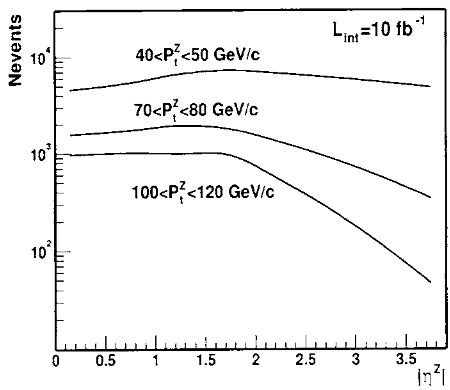

Fig. 5: η-dependence of rates for different $P_t{}^Z$ intervals.

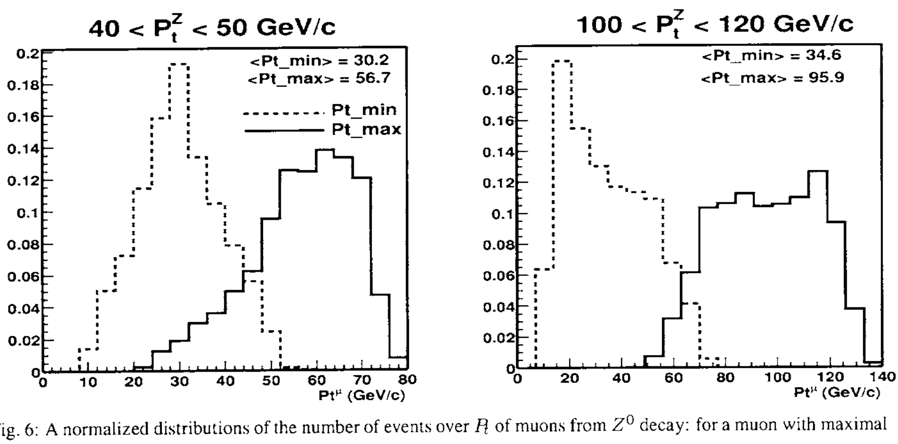

Fig. 6: A normalized distributions of the number of events over P_t of muons from Z^0 decay: for a muon with maximal P_t (full line) and for a muon with minimal P_t (dashed line) in the pair.

In Fig. 6 we have plotted a normalized distributions of the number of events over P_t of muons from Z^0 decay for two $P_t{}^Z$ intervals: $40 < P_t{}^Z < 50$ and $100 < P_t{}^Z < 120\; GeV/c$. The

[6]The analogous conclusion was done by studying "$\gamma + jet$" events in [12].

[7]We have limited Z^0 pseudorapidity spectrum from above in Fig. 5 and Table 8 only to give understanding about its behavior inside this η^Z interval and, certainly, have not used those limits as cuts anywhere in this paper.

muon spectra are limited by the condition (6) $P_t{}^{\mu} > 10\ GeV/c$. We also see that the spectra with muons having maximal P_t in the pair starts at $20\ GeV/c$ for $40 < P_t{}^Z < 50\ GeV/c$ and at $50\ GeV/c$ for $100 < P_t{}^Z < 120\ GeV/c$. It explains our choice in (6) for $P_{t\,max}^{\mu}$ restriction.

Table 8: The number of events for $L_{int} = 10\ fb^{-1}$ for different intervals of $P_t{}^Z$ and η^Z ($P_{t\,CUT}^{clust} = 10\ GeV/c$, $P_{t\,CUT}^{out} = 10\ GeV/c$ and $\Delta\phi \leq 15^\circ$).

$P_t{}^Z$	$\lvert\Delta\eta^Z\rvert$ intervals						all $\lvert\eta^Z\rvert$
(GeV/c)	0.0-0.5	0.5-1.0	1.0-1.5	1.5-2.0	2.0-2.5	2.5-5.0	0.0-5.0
40 – 50	4594	5425	6673	7267	6732	4796	35486
50 – 60	3128	3509	4297	4570	3976	2000	21471
60 – 70	2253	2443	2855	2934	2229	851	13567
70 – 80	1580	1734	1948	1786	1307	341	8692
80 – 90	1152	1148	1267	1236	824	170	5790
90 –100	741	859	812	808	523	59	3802
100 –110	582	590	594	546	305	36	2657
110 –120	384	428	451	412	226	8	1905
120 –140	523	582	562	531	293	12	2503
140 –170	392	380	368	341	190	4	1675
170 –200	170	186	162	170	63	2	756
200 –240	111	103	99	91	40	0	444
240 –300	71	51	44	48	20	0	238

3.3 Estimation of "$Z^0 + jet$" event rates for the Barrel, Endcap and Forward regions

Since a jet is a wide-spread object, we present the η^{jet} dependence of rates (for different $P_t{}^Z$ intervals) in a different way. Namely, Tables 9 and 10 include the rates of events (at $L_{int} = 10\ fb^{-1}$) for different η^{jet} intervals, covered by the Barrel, Endcap and Forward (HB, HE and HF) parts of the calorimeter. The events are selected after the cuts (5) – (13) (Selection 1) with the following values of the cut parameters:

$$\Delta\phi < 15^\circ, \quad P_{t\,CUT}^{clust} = 10\ GeV/c, \quad P_{t\,CUT}^{out} = 10\ GeV/c. \tag{23}$$

The first columns of these tables give the number of events with jets (found by the LUCELL jetfinding algorithm of PYTHIA), all particles of which are comprised entirely (100%) in the Barrel part (HB) and there is a 0% sharing ($\Delta P_t{}^{jet} = 0$) of $P_t{}^{jet}$ between the HB and the neighboring HE part of the calorimeter. The second columns of the tables contain the number of events in which P_t of the jet is shared between the HB and HE regions. The same sequence of restriction conditions takes place in the next columns. Thus, the HE and HF columns include the number of events with jets entirely contained in these regions, while the HE+HF column gives the number of events where the jet covers both the HE and HF regions. From these tables we can see what number of events can, in principle, be suitable for the most precise jet energy calibration procedure, carried out separately for the HB, HE and HF parts of the calorimeter in different $P_t{}^Z (\approx P_t{}^{jet})$ intervals. Less restrictive conditions, when up to 10% of the jet P_t are allowed to be shared between the HB, HE and HF parts of the calorimeter, are given in Tables 9 and 10 that correspond to the case of Selection 1.

Table 9: Selection 1. $\Delta {P_t}^{jet}/{P_t}^{jet} = 0.00$ (L_{int}=10 fb^{-1}).

${P_t}^Z$	HB	HB+HE	HE	HE+HF	HF
40 – 50	15072	11179	5417	3045	729
50 – 60	9076	7037	3231	1734	376
60 – 70	5813	4447	2055	1030	218
70 – 80	3726	2903	1275	669	123
80 – 90	2542	1901	847	432	67
90 – 100	1711	1243	558	246	44
100 – 110	1263	879	352	150	12
110 – 120	836	681	289	107	20
120 – 140	1085	836	400	154	8
140 – 170	752	626	218	71	8
170 – 200	348	261	103	44	0
200 – 240	206	139	75	20	0
240 – 300	111	95	28	4	0
40 – 300	44554	34076	15789	8510	2020

Table 10: Selection 1. $\Delta {P_t}^{jet}/{P_t}^{jet} \leq 0.10$ (L_{int}=10 fb^{-1}).

${P_t}^Z$	HB	HB+HE	HE	HE+HF	HF
40 – 50	19610	3251	10328	887	1366
50 – 60	12161	1667	6439	420	768
60 – 70	7797	950	4166	202	444
70 – 80	5077	570	2633	162	253
80 – 90	3453	372	1734	83	147
90 – 100	2261	242	1152	48	95
100 – 110	1683	170	729	32	40
110 – 120	1176	87	582	16	45
120 – 140	1465	139	816	36	43
140 – 170	1026	115	511	12	12
170 – 200	475	48	222	5	8
200 – 240	273	17	147	3	4
240 – 300	158	15	59	0	0
40 – 300	59392	8169	31395	2127	3861

Our estimation has shown that the requirement of jet isolation with $\epsilon^{jet} < 5\%$ (see (13)) would lead to about twofold reduction of the number of events.

From the last summarizing line of Table 9 we see that for the whole interval $40 < Pt^Z < 300$ GeV/c PYTHIA predicts about 45 000 events for HB, 16 000 events for HE and about 2 000 events for HF at L_{int}=10 fb^{-1}.

4. Dependence of the imbalance between P_t^Z and P_t^{jet} on the P_{tCUT}^{clust} and P_{tCUT}^{out} parameters

Here we shall study in detail a dependence of the $P_t^Z - P_t^{jet}$ imbalance on the values of P_{tCUT}^{clust} and P_{tCUT}^{out}. For this aim the four samples of "$Z^0 + jet$" events described in the beginning of Section 3 were used.

The mean values of the most important variables used in our analyses that reflect the main features of "$Z^0 + jet$" events (P_t56, $\Delta\phi$, P_t^{out}, $P_t^{\eta>5}$, $(P_t^Z - P_t^{part})/P_t^Z$ and $(P_t^J - P_t^{part})/P_t^J$) with the jet completely contained in the Barrel region, i.e. "HB events" (see Section 3.3) may be found in Appendices to [22].

Here our analysis is concentrated on the events with jets (as well as clusters) found by LUCELL jetfinder in the whole η region $|\eta^{jet}| < 5.0$. The influence of a wide variation of cuts P_{tCUT}^{clust} and P_{tCUT}^{out} on
(a) the number of selected events (for $L_{int} = 10\,fb^{-1}$),
(b) the mean value of $F \equiv (P_t^Z - P_t^{jet})/P_t^Z$ and
(c) the standard deviation value $\sigma(F)$
is presented in Tables 1–9 for Selection 1 of Appendix. The set of selection cuts (4)–(10) (Section 2.2) was applied to preselect "$Z^0 + jet$" events for the tables of Appendix.

Tables 1–3 of Appendix correspond to the "$Z^0 + jet$" events selection in the interval of $40 \leq P_t^Z \leq 70\ GeV/c$ Tables 4–6 to that for $70 \leq P_t^Z \leq 100\ GeV/c$ and Tables 7–9 to that for $100 \leq P_t^Z \leq 140\ GeV/c$.

We see that the restriction of P_t^{clust} and P_t^{out} are necessary to improve the jet energy setting accuracy. So, Tables 2 (for $40 \leq P_t^Z \leq 70\ GeV/c$) and 8 (for $100 \leq P_t^Z \leq 140\ GeV/c$) of Appendix show that the mean values of the fraction $F \equiv (P_t^Z - P_t^{jet})/P_t^Z$ decreases with variation of the two cuts from $P_{tCUT}^{clust} = 30\ GeV/c$ and $P_{tCUT}^{out} = 1000\ GeV/c$ (i.e. without limits) to $P_{tCUT}^{clust} = 10\ GeV/c$ and $P_{tCUT}^{out} = 10\ GeV/c$ as 0.049 to 0.018 and as 0.036 to 0.012, respectively. At the same time this restriction noticeably decreases the width of the Gaussian $\sigma(F)$ (see Tables 3, 6 and 9 of Appendix). So, it drops from 0.200 to 0.103 for $40 \leq P_t^Z \leq 70\ GeV/c$ and from 0.138 to 0.066 for $100 \leq P_t^Z \leq 140\ GeV/c$ for the same variation of P_{tCUT}^{clust} and P_{tCUT}^{out}.

Again, the reason is caused by the term $P_t(O + \eta > 5)/P_t^Z$ of the P_t-balance equation (19) (as we noted above, the contribution of $(1 - cos\Delta\phi)$ to the $P_t^Z - P_t^{jet}$ imbalance is negligibly small). This term can be decreased by decreasing P_t activity in the space *out of* the "$Z^0 + jet$" system, i.e. by limiting P_t^{clust} and P_t^{out}.

The numbers of events at the integrated luminosity $L_{int} = 10\,fb^{-1}$ for different P_{tCUT}^{clust} and P_{tCUT}^{out} are given in Tables 1, 5 and 9 of Appendix. One can see that even with such strict P_{tCUT}^{clust} and P_{tCUT}^{out} values as $10\ GeV/c$ for both, for example, we would have 69 600, 18 100 and 6 860 for $40 \leq P_t^Z \leq 70\ GeV/c$, $70 \leq P_t^Z \leq 100\ GeV/c$ and $100 \leq P_t^Z \leq 140\ GeV/c$ respectively.

The information analogous to that in Tables 1–12 for the events selected after imposing the jet isolation requirement may be found in [22].

The behavior of number of the selected events for $L_{int} = 10\,fb^{-1}$, the mean values of $(P_t^Z - P_t^{jet})/P_t^Z$ and its standard deviation $\sigma(F)$ as a function of P_{tCUT}^{out} for $P_{tCUT}^{clust} = 20\ GeV/c$ is displayed in Fig. 7 for events with non-isolated (left-hand column) and isolated jets (right-hand column) with $\epsilon^{jet} = 8\%$ at $40 \leq P_t^Z \leq 70\ GeV/c$ and $\epsilon^{jet} = 5\%$ at

$70 \leq {P_t}^Z \leq 100\ GeV/c$ and $100 \leq {P_t}^Z \leq 140\ GeV/c$. From the middle plot of the right-hand column we see that one can obtain a much better fractional balance F, less than 1% for all ${P_t}^Z$ intervals. As in the case of events with non-isolated jets, the restriction of upper cut on ${P_t}^{out}$ also lead to improving the systematic uncertainty, i.e. decreasing $\sigma(F)$.

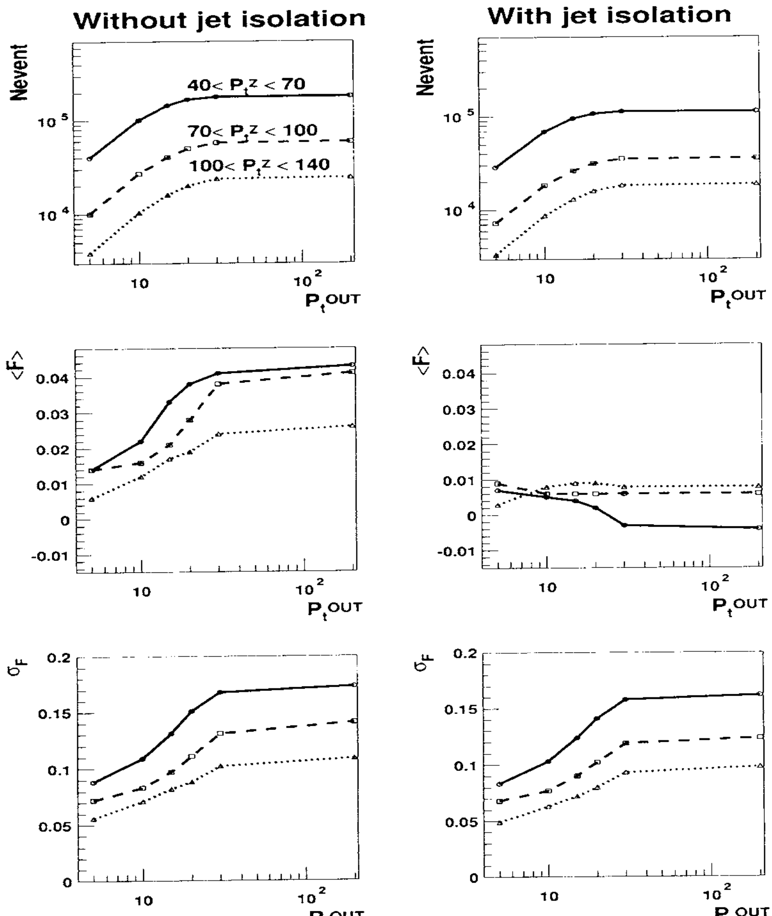

Fig. 7: Number of events at $L_{int} = 10\ fb^{-1}$, mean value of $F \equiv ({P_t}^Z - {P_t}^{jet})/{P_t}^Z$ ($< F >$), its standard deviation (σ_F) as a function of P_{tCUT}^{out} value. P_{tCUT}^{clust} value is limited by $20\ GeV/c$. Full line corresponds to the event selection with $40 \leq {P_t}^Z \leq 70\ GeV/c$, dashed line to that with $70 \leq {P_t}^Z \leq 100\ GeV/c$ and dotted line to that with $100 \leq {P_t}^Z \leq 140\ GeV/c$ ($\epsilon^{jet} = 8\%, 5\%, 5\%$ in these ${P_t}^Z$ intervals, respectively).

Appendix

$$40 \leq P_t^Z \leq 70 \;\; GeV/c$$

Table 11: Number of events per $L_{int} = 10 \; fb^{-1}$.

$P_{t\,max}^{clust}$ (GeV/c)	$P_{t\,max}^{out}$ (GeV/c)					
	5	10	15	20	30	1000
5	9700	17700	19200	19300	19300	19300
10	30700	69600	87300	91700	92400	92400
15	37700	92600	127400	141500	146600	146900
20	40000	100900	145400	167700	179200	180300
30	41400	106600	157600	187100	208900	213100

Table 12: $\langle F \rangle$, $F = ({P_t}^Z - {P_t}^{jet})/{P_t}^Z$.

$P_{t\,max}^{clust}$ (GeV/c)	$P_{t\,max}^{out}$ (GeV/c)					
	5	10	15	20	30	1000
5	0.014	0.015	0.016	0.016	0.016	0.016
10	0.013	0.018	0.023	0.024	0.024	0.024
15	0.014	0.021	0.029	0.033	0.034	0.034
20	0.014	0.022	0.033	0.038	0.041	0.041
30	0.014	0.023	0.034	0.042	0.047	0.049

Table 13: $\sigma(F)$, $F = ({P_t}^Z - {P_t}^{jet})/{P_t}^Z$.

$P_{t\,max}^{clust}$ (GeV/c)	$P_{t\,max}^{out}$ (GeV/c)					
	5	10	15	20	30	1000
5	0.079	0.088	0.093	0.094	0.095	0.095
10	0.085	0.103	0.115	0.121	0.124	0.124
15	0.086	0.107	0.126	0.140	0.150	0.151
20	0.088	0.109	0.131	0.151	0.168	0.173
30	0.088	0.110	0.134	0.158	0.187	0.200

$70 \leq {P_t}^Z \leq 100 \ GeV/c$

Table 14: Number of events per $L_{int} = 10 \ fb^{-1}$.

${P_t}^{clust}_{max}$ (GeV/c)	${P_t}^{out}_{max}$ (GeV/c) 5	10	15	20	30	1000
5	2500	4500	4900	5000	5000	5000
10	7600	18100	23000	24800	25200	25200
15	9500	24700	35000	40700	43900	44000
20	10100	27000	40300	50000	57900	59200
30	10600	28700	44500	57900	73200	79200

Table 15: $\langle F \rangle$, $F = ({P_t}^Z - {P_t}^{jet})/{P_t}^Z$.

${P_t}^{clust}_{max}$ (GeV/c)	${P_t}^{out}_{max}$ (GeV/c) 5	10	15	20	30	1000
5	0.011	0.012	0.012	0.012	0.013	0.013
10	0.012	0.013	0.015	0.018	0.018	0.018
15	0.013	0.015	0.019	0.024	0.028	0.029
20	0.014	0.016	0.021	0.028	0.038	0.043
30	0.014	0.017	0.023	0.033	0.050	0.066

Table 16: $\sigma(F)$, $F = ({P_t}^Z - {P_t}^{jet})/{P_t}^Z$.

${P_t}^{clust}_{max}$ (GeV/c)	${P_t}^{out}_{max}$ (GeV/c) 5	10	15	20	30	1000
5	0.069	0.070	0.074	0.075	0.077	0.077
10	0.071	0.078	0.088	0.093	0.095	0.096
15	0.071	0.082	0.094	0.105	0.116	0.118
20	0.072	0.083	0.097	0.111	0.131	0.141
30	0.073	0.084	0.100	0.118	0.149	0.178

$$100 \leq P_t^Z \leq 140 \;\; GeV/c$$

Table 17: Number of events per $L_{int} = 10 \; fb^{-1}$.

$P_{t\,max}^{clust}$ (GeV/c)	$P_{t\,max}^{out}$ (GeV/c)					
	5	10	15	20	30	1000
5	930	1710	1890	1920	1920	1920
10	3000	6860	9010	9660	9910	9930
15	3660	9320	13750	16110	17700	17910
20	3880	10320	15950	19880	23600	24330
30	4050	10970	17470	22910	30640	34110

Table 18: $\langle F \rangle$, $F = (P_t{}^Z - P_t{}^{jet})/P_t{}^Z$.

$P_{t\,max}^{clust}$ (GeV/c)	$P_{t\,max}^{out}$ (GeV/c)					
	5	10	15	20	30	1000
5	0.007	0.006	0.009	0.008	0.008	0.008
10	0.005	0.012	0.014	0.014	0.015	0.015
15	0.005	0.011	0.015	0.017	0.018	0.019
20	0.006	0.012	0.017	0.019	0.024	0.026
30	0.005	0.013	0.017	0.022	0.033	0.036

Table 19: $\sigma(F)$, $F = (P_t{}^Z - P_t{}^{jet})/P_t{}^Z$.

$P_{t\,max}^{clust}$ (GeV/c)	$P_{t\,max}^{out}$ (GeV/c)					
	5	10	15	20	30	1000
5	0.046	0.045	0.050	0.051	0.050	0.050
10	0.054	0.066	0.075	0.076	0.080	0.080
15	0.054	0.068	0.079	0.084	0.092	0.095
20	0.056	0.071	0.082	0.088	0.102	0.109
30	0.055	0.073	0.084	0.092	0.113	0.138

Acknowledgments

We are greatly thankful to D. Denegri for having offered this theme to study, fruitful discussions and permanent support and encouragement. It is a pleasure for us to express our recognition for helpful discussions to P. Aurenche, M. Dittmar, M. Fontannaz, J.Ph. Guillet, M.L. Mangano, E. Pilon, H. Rohringer, S. Tapprogge and especially to J. Womersley for supplying us with the preliminary version of paper [1].

References

[1] D0 Collaboration, F. Abachi *et al.*, NIM **A424** (1999)352.

[2] CDF Collaboration. F. Abe *et al.*, Phys.Rev. **D50** (1994)2966; F. Abe *et al.*, Phys.Rev.Lett. **73** (1994)225.

[3] D. Denegri, R. Kinnunen, A. Nikitenko, CMS Note 1997/039 "Study of calorimeter calibration with τ's in CMS".

[4] R. Kinnunen, A. Nikitenko, CMS Note 1997/097 "Study of calorimeter calibration with pions from jets in CMS".

[5] J. Womersley, A talk at CMS physics group meeting at CMS Week, Aachen, 1996. See also http://cmsdoc.cern.ch/doc/gen/agendas/960908-1.

[6] J. Freeman, W. Wu, **draft** "In situ calibration of CMS HCAL calorimeter".

[7] R. Mehdiyev, I. Vichou, ATLAS Note ATL-COM-PHYS-99-054 (1999) "Hadronic jet energy scale calibration using Z+jet events".

[8] P. Savard, ATLAS Note CAL-NO-092 (1997), "The $W \to jet + jet$ and top mass reconstructions with the ATLAS detector".

[9] ATLAS Detector and Physics Performance, Technical Design Report, Volumes **1, 2**, 1999. CERN/LHCC 99-14.

[10] N.B. Skachkov, V.F. Konoplyanikov, D.V. Bandourin, "Photon – jet events for calibration of HCAL". Second Annual RDMS CMS Collaboration Meeting. CMS-Document, 1996–213. CERN, December 16-17, 1996, p.7-23.

[11] N.B. Skachkov, V.F. Konoplyanikov, D.V. Bandourin, "γ-direct + 1 jet events for HCAL calibration". Third Annual RDMS CMS Collaboration Meeting. CMS-Document, 1997–168. CERN, December 16-17, 1997, p.139-153.

[12] D.V. Bandourin, V.F. Konoplyanikov, N.B. Skachkov. "Jet energy scale setting with "$\gamma + jet$" events at LHC energies. Generalities, selection rules." JINR Preprint E2-2000-251, JINR, Dubna, hep-ex/0011012.

[13] D.V. Bandourin, V.F. Konoplyanikov, N.B. Skachkov. "Jet energy scale setting with "$\gamma + jet$" events at LHC energies. Event rates, P_t structure of jet." JINR Preprint E2-2000-252, JINR, Dubna, hep-ex/0011013.

[14] D.V. Bandourin, V.F. Konoplyanikov, N.B. Skachkov. "Jet energy scale setting with "$\gamma + jet$" events at LHC energies. Minijets and cluster suppression and ${P_t}^{\gamma} - {P_t}^{Jet}$ disbalance." JINR Preprint E2-2000-253, JINR, Dubna, hep-ex/0011084.

[15] D.V. Bandourin, V.F. Konoplyanikov, N.B. Skachkov. "Jet energy scale setting with "$\gamma + jet$" events at LHC energies. Selection of events with a clean "$\gamma + jet$" topology and ${P_t}^{\gamma} - {P_t}^{Jet}$ disbalance." JINR Preprint E2-2000-254, JINR, Dubna, hep-ex/0011014.

[16] D.V. Bandourin, V.F. Konoplyanikov, N.B. Skachkov. "Jet energy scale setting with "$\gamma + jet$" events at LHC energies. Detailed study of the background suppression." JINR Preprint E2-2000-255, JINR, Dubna, hep-ex/0011017.

[17] CMS Muon Project, Technical Design Report, CERN/LHCC 97–32, CMS TDR 3, CERN, 1997.

[18] T. Sjostrand, Comp.Phys.Comm. **82** (1994)74.

[19] S. Abdullin, A. Khanov, N. Stepanov, CMS Note CMS TN/94–180 "CMSJET".

[20] D.V. Bandourin, V.F. Konoplyanikov, N.B. Skachkov, " "$\gamma + jet$" events rate estimation for gluon distribution determination at LHC", Part.Nucl.Lett.**103**:34-43,2000, hep-ex/0011015.

[21] D.V. Bandourin, N.B. Skachkov. " "$\gamma + jet$" process application for setting the absolute scale of jet energy and determining the gluon distribution at the Tevatron Run II." D0 Note 3948, 2002.

[22] D.V. Bandourin, N.B. Skachkov. "On the application of Z^0+jet events for setting the absolute jet energy scale and determining the gluon distribution in a proton at the LHC", 2002, hep-ex/0209039.

Received on August 14, 2003.

Бандурин Д. В., Скачков Н. Б. E1-2003-163
Установление шкалы энергии струи
с помощью событий «Z^0+струя» на LHC

Изучается возможность установления шкалы энергии струи с помощью процесса $pp \to Z^0 + \text{jet} + X$ на LHC. Демонстрируется влияние нового набора критериев, предложенных в наших предыдущих работах, на улучшение баланса $P_t^Z - P_t^{\text{jet}}$. Представлены распределения числа событий по P_t^Z и η^{jet}.

Работа выполнена в Лаборатории ядерных проблем им. В. П. Джелепова ОИЯИ.

Сообщение Объединенного института ядерных исследований. Дубна, 2003

Bandurin D. V., Skachkov N. B. E1-2003-163
Setting the Absolute Scale of Jet Energy
with «Z^0+jet» Events at LHC

A possibility of jet energy scale setting by help of $pp \to Z^0 + \text{jet} + X$ process at LHC is studied. The effect of new set of cuts, proposed in our previous works, on the improvement of the $P_t^Z - P_t^{\text{jet}}$ balance is demonstrated. The distributions of the selected events over P_t^Z and η^{jet} are presented.

The investigation has been performed at the Dzhelepov Laboratory of Nuclear Problems, JINR.

Communication of the Joint Institute for Nuclear Research. Dubna, 2003

Корректор *Т. Е. Попеко*

Подписано в печать 09.12.2003.
Формат 60 × 90/16. Бумага офсетная. Печать офсетная.
Усл. печ. л. 1,43. Уч.-изд. л. 2,35. Тираж 365 экз. Заказ № 54209.

Издательский отдел Объединенного института ядерных исследований
141980, г. Дубна, Московская обл., ул. Жолио-Кюри, 6.
E-mail: publish@pds.jinr.ru
www.jinr.ru/publish/